JACS
JOURNAL OF THE AMERICAN CHEMICAL SOCIETY
Article
pubs.acs.org/JACS

Turning Gold into "Diamond": A Family of Hexagonal Diamond-Type Au-Frameworks Interconnected by Triangular Clusters in the Sr–Al–Au System

Andriy Palasyuk,[†] Yuri Grin,[‡] and Gordon J. Miller*[,†]

[†]Department of Chemistry, Iowa State University, Ames, Iowa 50011
[‡]Max-Planck-Institut für Chemische Physik fester Stoffe, Dresden, Germany

Supporting Information

ABSTRACT: A new homologous series of intermetallic compounds containing three-dimensional (3-d) tetrahedral frameworks of gold atoms, akin to hexagonal diamond, have been discovered in four related Sr–Au–Al systems: (**I**) hexagonal $SrAl_{3-x}Au_{4+x}$ ($0.06(1) \le x \le 0.46(1)$, $P\bar{6}2m$, $Z = 3$, $a = 8.633(1)-8.664(1)$ Å, $c = 7.083(2)-7.107(1)$ Å); (**II**) orthorhombic $SrAl_{2-y}Au_{5+y}$ ($y \le 0.05(1)$; *Pnma*, $Z = 4$, $a = 8.942(1)$ Å, $b = 7.2320(4)$ Å, $c = 9.918(1)$ Å); (**III**) $Sr_2Al_{2-z}Au_{7+z}$ ($z = 0.32(2)$; $C2/c$, $Z = 4$, $a = 14.956(4)$ Å, $b = 8.564(2)$ Å, $c = 8.682(1)$ Å, $\beta = 123.86(1)°$); and (**IV**) rhombohedral $Sr_2Al_{3-w}Au_{6+w}$ ($w \approx 0.18(1)$; $R\bar{3}c$, $Z = 6$, $a = 8.448(1)$ Å, $c = 21.735(4)$ Å). These remarkable compounds were obtained by fusion of the pure elements and were characterized by X-ray diffraction and electronic structure calculations. Phase **I** shows a narrow phase width and adopts the $Ba_3Ag_{14.6}Al_{6.4}$-type structure; phase **IV** is isostructural with $Ba_2Au_6Zn_3$, whereas phases **II** and **III** represent new structure types. This novel series can be formulated as $Sr_x[M_3]_{1-x}Au_2$, in which $[M_3]$ (= $[Al_3]$ or $[Al_2Au]$) triangles replace some Sr atoms in the hexagonal prismatic-like cavities of the Au network. The $[M_3]$ triangles are either isolated or interconnected into zigzag chains or nets. According to tight-binding electronic structure calculations, the greatest overlap populations belong to the Al–Au bonds, whereas Au–Au interactions have a substantial nonbonding region surrounding the calculated Fermi levels. QTAIM analysis of the electron density reveals charge transfer from Sr to the Al–Au framework in all four systems. A study of chemical bonding by means of the electron-localizability indicator indicates two- and three-center interactions within the anionic Al–Au framework.

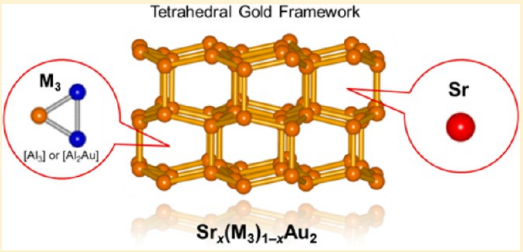

INTRODUCTION

A rapidly growing class of metal-rich solids belongs to *polar intermetallic compounds*,[1] which involve combinations of an electropositive metal among the first three groups of the Periodic Table with electronegative, late- or post-transition metals. The "polar" designation refers to the formal electron transfer from the active metal component to the electronegative ones according to their electronegativity differences, whereas the intrinsic metallic nature of these compounds requires electron back-donation from the electronegative to the electropositive component. Thus, there is no significant overall net charge transfer but, rather, a redistribution of the occupied valence states of the constituent elements. This fundamental aspect of their electronic structures and the breadth of chemical elements that are available to form polar intermetallics leads to a broad range of complex structural chemistry and potential physical properties, such as superconductivity, thermoelectric behavior, and itinerant or local magnetism, all of which create systems that are ripe for exploration, analysis, and application.

As a compound class, polar intermetallics lie between two classical intermetallic families: Zintl–Klemm (ZK) phases[2−5] and Hume–Rothery (HR) phases.[6,7] ZK phases are valence compounds also involving electropositive and electronegative elements in which the latter form polyanions using all available valence electrons to form typically two-center, two-electron bonds or, in some cases, deltahedral clusters according to the Wade–Mingos rules.[8,9] HR phases, on the other hand, involve densely packed late- and post-transition metals with structures that follow specific valence electron-to-atom (e/a) ratios.[10] In polar intermetallic compounds, the electronegative metals adopt structures that generally optimize polar-covalent bonds, as in ZK phases, according to analysis of their electronic structures, but their atomic structures usually involve significant multicentered, delocalized bonding, as observed in HR phases.[1] In particular, inclusion of late transition metals T with formally filled $4d$ or $5d$ shells, i.e., T = Pd–Cd or Pt–Hg, with the heavier trielide or tetrelide elements (X = Ga, In, Tl; Ge, Sn) and the active alkali or alkaline earth metals (A) has revealed numerous compounds with great stoichiometric and structural variety, e.g., polyanionic networks with complex polyhedral cavities or tunnels filled by cations,[11−20] as well as icosahedral quasicrystals and approximants.[21]

Received: October 31, 2013
Published: January 31, 2014

dx.doi.org/10.1021/ja411150e | J. Am. Chem. Soc. 2014, 136, 3108−3117

Table 1. Single Crystal and Refinement Data for I ($SrAl_{2.94}Au_{4.06(1)}$), II ($SrAl_{1.95}Au_{5.05(1)}$), III ($Sr_2Al_{1.67}Au_{7.32(2)}$), and IV ($Sr_2Al_{2.82}Au_{6.18(1)}$)[a]

crystal	I	II	III	IV
formula mass	967.19	1135.34	1663.21	1469.14
space group; Z	$P\bar{6}2m$; 3	$Pnma$; 4	$C2/c$; 4	$R\bar{3}c$; 6
a (Å)	8.633(1)	8.942(1)	14.956(4)	8.448(1)
b (Å)		7.2320(4)	8.564(2)	
c (Å)	7.083(2)	9.918(1)	8.672(1)	21.735(4)
β (deg)			123.860(7)	
V (Å^3)	457.2(1)	641(1)	922.4(3)	1343.2(4)
d_c (Mg/m^3)	10.54	11.75	11.98	10.90
μ (mm^{-1}; Mo Kα)	106.4	123.5	127.6	112.9
reflns collected/R_{int}	2870/0.068	3653/0.056	4673/0.062	11367/0.11
ind. data/restraints/params	276/0/29	841/0/41	1153/0/53	732/0/20
GoF (F^2)	1.154	1.121	1.172	1.178
$R1/wR2$ [$I > 2\sigma(I)$]	0.0239/0.0520	0.0193/0.0448	0.0469/0.1035	0.0449/0.0515
$R1/wR2$ [all data]	0.0257/0.0529	0.0223/0.0457	0.0583/0.1076	0.0981/0.1003
largest diff peak/hole (e/Å^3)	1.97/−1.56	1.76/−1.67	2.73/−2.73	2.79/−2.81

[a]Similar information for **I*** ($SrAl_{2.54}Au_{4.46(1)}$) is listed in Table S2 of SI.

Among the variety of new $A-T-X$ phases, the greatest successes for the discovery and subsequent characterization of complex polar intermetallics have emerged for T = Pt[22−24] and Au.[25−38] These two late transition metals show substantial relativistic effects on their valence 6*s* electrons (and orbital).[39] This relativistic effect causes Pt and Au to have electronegativities on par with chalcogenides like Se and Te,[40] as well as enhances the ability of the valence 5*d* electrons (and orbitals) to engage in bonding with various metals.[41] In particular, a wide variety of Au motifs have been observed, including chains or sheets of condensed Au_4 tetrahedra,[32] wavy layers,[30] hexagonal stars,[33] squares,[34] as well as a new quasicrystal[35] and crystalline approximants.[36] The calculated electronic density of states (DOS) of these compounds often indicate pseudogaps around the Fermi level, an outcome which is a partial signature of electronic stability because this feature frequently separates filled bonding states below from empty antibonding states above the pseudogap. Although the strongest orbital interactions are the heteroatomic Au−X contacts, which, together with Au−Au interactions, typically constitute ∼40−65% of the total Hamilton population from all near-neighbor pairwise contacts, an increasing role of A−Au bonding has become evident because they achieve, in some cases,[26−28] up to ∼25% of the total Hamilton population.

In this work, we have extended the search for novel polar intermetallic compounds into the largely unexplored phase spaces of Ae−Au−Al systems (Ae = alkaline earth metals). The choice of Al as the trielide component, in contrast to Ga−Tl, is motivated by its location in the Periodic Table on the *amphoteric*, or *metalloid* line, an observation which implies that the chemistry of Al-containing intermetallic compounds may be different from the chemistry of the other triels. In particular, additional structure-bonding relationships that could facilitate a better general understanding of the compositions and stabilities of polar intermetallics are anticipated. On the other hand, new kinds of Au-clustering or Au-frameworks are anticipated in Ae−Au−Al systems, because of significant chemical differences between Al and the other triels. The fact that Al is one of most abundant chemical elements on earth, and is extensively present in modern technology, runs counter to the meager list of Ae−Au−Al representatives found in the ICSD database.[42−45]

In the present work, we report structural and bonding analyses of four new examples from the Sr−Al−Au system: (**I**) hexagonal $SrAl_{2.94}Au_{4.06(1)}$; (**II**) orthorhombic $SrAl_{1.95}Au_{5.05(1)}$; (**III**) monoclinic $Sr_2Al_{1.67}Au_{7.32(2)}$; and (**IV**) rhombohedral $Sr_2Al_{2.82}Au_{6.18(1)}$ (hereafter termed as $SrAl_{3-x}Au_{4+x}$, $SrAl_{2-y}Au_{5+y}$, $Sr_2Al_{2-z}Au_{7+z}$, and $Sr_2Al_{3-w}Au_{6+w}$, respectively). We are expressing chemical formulas of these Sr−Al−Au phases in increasing order of absolute electronegativities. These four compounds, indeed, now represent the first examples of a completely new homologous series that are united by a common unique structural and bonding feature for Au atoms: a hexagonal diamond-like framework.

EXPERIMENTAL SECTION

Syntheses. High purity starting reagents included dendritic Sr (99.9%, Alfa-Aesar), Au ingots (99.997%, Ames Lab), and Al ingots (99.999%, Alfa-Aesar). These were handled in a N_2-filled glovebox in which the moisture level was maintained below 0.1 ppm (by volume). The surfaces of strontium and aluminum were cut clean with a scalpel just before use. The reactions were carried out in welded Ta metal tubing jacketed within evacuated fused silica containers and heated in resistance furnaces.[46] All reactions were run at 1000 °C for 24h, then slowly (5 °C/h) cooled to 750 °C, annealed at that temperature for 72h, and finally quenched in cold water. Phase purity was assessed by comparison of the experimental powder X-ray diffraction (PXRD) patterns with those calculated from structures refined from single crystal XRD. All products are not terribly sensitive to exposure to air; several weeks of exposure are needed to detect slight changes in product appearances. Nevertheless, all manipulations of the products minimized their exposure to air.

Powder X-ray Diffraction. Powder diffraction data were collected at 293(2) K using a Huber 670 Guinier powder camera equipped with an area detector and Cu Kα radiation (λ = 1.540598 Å). In a glovebox, powdered samples were homogeneously dispersed between two Mylar sheets with the aid of a little vacuum grease. These were, in turn, held between split Al rings that provided airtight seals. Unit cell parameters were refined using the WinXPow program.[47]

Structure Determinations. Single crystal diffraction data were obtained at 293(2) K using Mo K_α radiation (λ = 0.71073 Å) and a Bruker SMART APEX CCD diffractometer. The data were collected in the form of three sets of 606 frames with 0.3° scans in ω and exposure times of 10 s per frame. Reflection intensities were integrated and corrected for Lorentz and polarization effects with the *SAINT* program in the *SMART* software package.[48] Space group determinations were accomplished using the *XPREP* program and the

dx.doi.org/10.1021/ja411150e | J. Am. Chem. Soc. 2014, 136, 3108−3117

Table 2. Atomic Coordinates, Equivalent Isotropic Displacement Parameters (Å^2 × 10^3), and Site Occupancy Factors Refined for I ($SrAl_{3.94}Au_{4.06(1)}$), II ($SrAl_{1.95}Au_{5.05(1)}$), III ($Sr_2Al_{1.67}Au_{7.32(2)}$), and IV ($Sr_2Al_{2.82}Au_{6.18(1)}$)[a]

	atom	Wyckoff site	x	y	z	U_{eq}	SOF (≠ 1)
I	Sr1	1*a*	0	0	0	9(2)	
	Sr2	2*d*	1/3	2/3	1/2	9(1)	
	Au1	6*i*	0.7065(1)	0	0.2975(2)	9(1)	
	Au2	6*i*	0.3729(1)	0	0.2050(1)	10(1)	
	M[b]	6*j*	0.2988(1)	0.4733(9)	0	16(3)	0.968(6) Al
	Al	3*g*	0.203(1)	0	1/2	10(3)	
II	Sr	4*c*	0.2540(2)	1/4	0.6243(2)	10(1)	
	Au1	8*d*	0.05381(6)	0.03935(7)	0.36424(5)	10(1)	
	Au2	8*d*	0.89164(6)	0.94359(7)	0.10215(5)	9(1)	
	Au3	4*c*	0.29654(8)	1/4	0.24296(7)	10(1)	
	M[b]	4*c*	0.1502(5)	3/4	0.4853(4)	11(2)	0.948(4) Al
	Al	4*c*	0.0525(6)	1/4	0.1192(6)	10(2)	
III	Sr	8*f*	0.1468(3)	0.2392(4)	0.2142(4)	14(1)	
	Au1	8*f*	0.2226(1)	0.0795(2)	0.9595(2)	14(1)	
	Au2	8*f*	0.1094(1)	0.1264(2)	0.5496(2)	15(1)	
	Au3	8*f*	0.4211(1)	0.9491(2)	0.0457(2)	16(1)	
	M1[b]	4*e*	0	0.0791(2)	3/4	15(1)	0.96(1) Au
	M2[b]	8*f*	0.4088(4)	0.1570(6)	0.2529(7)	16(1)	0.82(1) Al
IV	Sr	12*c*	0	0	0.0896(1)	10(1)	
	Au	36*f*	0.3510(1)	0.0386(1)	0.0152(1)	11(1)	
	M[b]	18*e*	0.1845(7)	0	1/4	15(2)	0.939(6) Al

[a]Similar information for **I*** ($SrAl_{2.54}Au_{4.46(1)}$) is listed in Table S3 of SI. [b]The atomic symbol "M" stands for Al/Au mixed occupancy.

SHELXTL 6.1 software package.[49] Empirical absorption corrections for all compounds were carried out using the *SADABS* program.[50] Finally, each structure was solved by direct methods using *SHELXTL* 6.1 and refined by full-matrix, least-squares fitting on F_o^2, ultimately with anisotropic displacement parameters and a secondary extinction parameter.

Electronic Structure Calculations. Electronic structure calculations and analysis of chemical bonding features were accomplished for the following ordered stoichiometric models using the lattice parameters and atomic coordinates from the corresponding crystal structure refinements of single-crystal X-ray diffraction data (see Tables 1 and 2): "$SrAl_3Au_4$" for **I** (position M is fully occupied with Al); "$SrAl_2Au_5$" for **II** (position M is fully occupied by Al); "$Sr_2Al_2Au_7$" for **III** (positions M1 and M2 are completely occupied by Au and Al, respectively); and "$Sr_2Al_3Au_6$' for **IV** (position M is completely occupied by Al). The TB-LMTO-ASA program package[51] was employed using the Barth-Hedin exchange potential[52] for the LDA calculations. The radial scalar-relativistic Dirac equation was solved to obtain the partial waves.[53] Because the calculation within the atomic sphere approximation (ASA) includes corrections for the neglect of interstitial regions and partial waves of higher order[54] an addition of empty spheres was not necessary. The following radii of the atomic spheres were applied for the calculations: "$SrAl_3Au_4$" (**I**), r(Sr1) = 2.285 Å, r(Sr2) = 2.386 Å, r(Al1) = 1.487 Å, r(Al2) = 1.452 Å, r(Au1) = 1.519 Å, r(Au2) = 1.495 Å; "$SrAl_2Au_5$" (**II**), r(Sr1) = 2.278 Å, r(Al1) = 1.500 Å, r(Al2) = 1.459 Å, r(Au1) = 1.542 Å, r(Au2) = 1.662 Å, r(Au3) = 1.513 Å; "$Sr_2Al_2Au_7$" (**III**), r(Sr1) = 2.209 Å, r(Al1) = 1.508 Å, r(Au1) = 1.540 Å, r(Au2) = 1.583 Å, r(Au3) = 1.543 Å, r(Au4) = 1.592 Å; and "$Sr_2Al_3Au_6$" (**IV**), r(Sr) = 2.224 Å, r(Al) = 1.500 Å, r(Au) = 1.527 Å. For each calculation, a basis set containing Sr(5*s*,4*d*), Au(6*s*,6*p*,5*d*) and Al(3*s*,3*p*) orbitals was employed with Sr(5*p*,4*f*), Au(4*f*) and Al(3*d*) functions being downfolded.[55] Meshes of 512 (8 × 8 × 8) k points in the irreducible parts of the corresponding first Brillouin zones were used to obtain density of states (DOS) and crystal orbital Hamilton population (COHP)[56] curves, and their subsequent integrated values.

The electron localizability indicator (ELI, Y) was evaluated in the ELI-D representation[57−59] with an ELI-D module within the TB-LMTO-ASA program package. Topological analysis of the electron density, i.e., estimation of the shapes, volumes, and charges of the atoms after Bader (quantum theory of atoms in molecules, QTAIM[60]), and of the electron localizability indicator, e.g., localization of the ELI maxima as fingerprints of the direct atomic interactions, was performed with the program DGrid.[61]

RESULTS AND DISCUSSION

Four distinct phases were obtained during systematic explorations in Sr-poor and Au-rich regions of the Sr−Al−Au system (see Figure 1). Well-formed single crystals of **I**, **II**, **III**, and **IV** were first obtained with at least 40%, 85%, 90%, and ∼95% (essentially single phase) yields from the reactions with loaded Sr:Al:Au molar ratios, respectively, of (1) 2:9:9; (2) 2:5:13; (3) 2:2:8; and (8) 2:3:6. According to powder X-ray

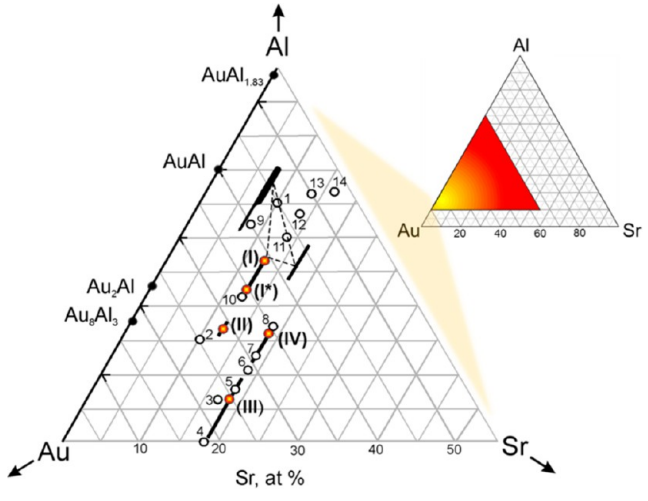

Figure 1. Section of the Sr−Au−Al diagram near the Au−Al binary line indicating reaction loadings (open circles) and emphasizing compounds characterized by single crystal and powder X-ray diffraction (**I**, **I***, **II**, **III**, and **IV**; filled circles).

dx.doi.org/10.1021/ja411150e | J. Am. Chem. Soc. 2014, 136, 3108−3117

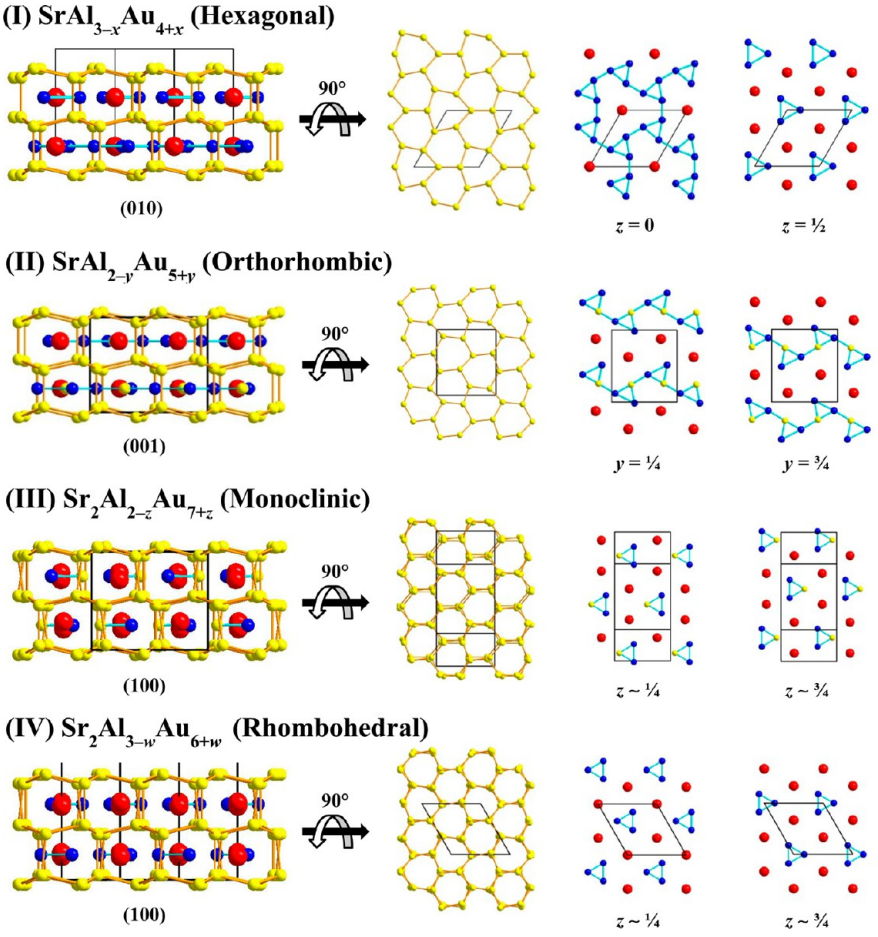

Figure 2. Analogous perspectives of the four crystal structures **I**, **II**, **III**, and **IV** and the two motifs described in the text; Sr (red), Au (yellow), Al or mixed Au/Al (blue). (Left) Perspective drawings emphasizing the hexagonal diamond type, tetrahedral framework of Au atoms with Sr atoms and M_3-triangles in the voids. (Right) Perspective drawings orthogonal to the planes of Sr atoms and M_3-triangles showing just the Au-net and the layers of Sr and M_3-triangles. On the left, for structures **I**, **II**, and **III**, complete unit cells are depicted; for **IV**, only one-third of the full rhombohedral cell in the hexagonal setting is shown.

diffraction, the phases $Sr(Al_{1-x}Au_x)_{12-13}$ ($NaZn_{13}$-type and related types)[62] and $Sr(Al_{1-x}Au_x)_5$ ($BaZn_5$-type)[63] formed alongside **I**, whereas the majority of Bragg reflections in the patterns of the products obtained from the latter three reaction loadings, which were Au-richer, fit well to simulations calculated from single crystal refinements, respectively, of **II**, **III**, and **IV**. A small number of low-intensity peaks that could not be assigned to these major phases were attributed to yet unidentified Au-richer compounds. Single-phase products of **I**, **II** and **III**, obtained in ~95% yields, were subsequently obtained when 1:2.6:4.4 (**I**), 1:2:5 (**II**), and (5) 2:2:7 (**III**) molar ratios were loaded (see X-ray powder diffraction patterns in Figure S1 of Supporting Information [SI]).

According to phase analysis from a combination of single crystal and powder X-ray diffraction experiments (see Table S1 of SI), the hexagonal phase **I** has a modest homogeneity width that can be described as $SrAl_{3-x}Au_{4+x}$ ($0.06(1) \le x \le 0.46(1)$). The upper bound was assessed by a comparison between the refined composition of a crystalline specimen **I*** ($SrAl_{2.54}Au_{4.46(1)}$), which was extracted from a Sr:Al:Au loading (9) 2:11:13, and the powder X-ray diffraction pattern from a sample loaded as "$SrAl_{2.5}Au_{4.5}$" (10), a pattern which showed ~85−90% of hexagonal $SrAl_{3-x}Au_{4+x}$ and ~10−15% of the Au-rich orthorhombic phase $SrAl_{2-y}Au_{5+y}$ (**II**). The presence of the orthorhombic phase **II** indicates a maximum Au content in the hexagonal phase $SrAl_{3-x}Au_{4+x}$ to be $x \approx 0.45(1)$. Additionally, least-squares refinement of unit cell parameters of the hexagonal phase in this powder X-ray diffraction pattern, i.e., $a = 8.660(2)$ and $c = 7.109(3)$, deviates less than 2σ from values obtained by single crystal refinement of specimen **I***. Therefore, the refined composition of **I***, $SrAl_{2.54}Au_{4.46(1)}$, represents the upper limit of Au content in the hexagonal $SrAl_{3-x}Au_{4+x}$ phase. The lower bound, $x \approx 0.06(1)$, could be assessed using similar reasoning for other loadings. Specimen **I**, which refined as $SrAl_{2.94}Au_{4.06(1)}$, must be close to the lower limit of Au content because crystals were selected from the three-phase product loaded as (1) 1:4.5:4.5.

The homogeneity widths of the other three compounds, **II**, **III**, and **IV**, were established following a similar analysis of X-ray powder diffraction patterns, single crystal experiments, and controlled loading patterns. Details of the analysis for these three phases are described in detail in SI.

Crystal Structures. Important crystallographic data for each phase **I**, **II**, **III**, and **IV** are summarized in Table 1, and their atomic positions, site occupancies, and equivalent isotropic displacement parameters are listed in Table 2. Important interatomic distances and more detailed crystallographic information, as well as anisotropic displacement parameters, are available from the corresponding CIF files, which are available in the SI.

dx.doi.org/10.1021/ja411150e | J. Am. Chem. Soc. 2014, 136, 3108−3117

Table 3. Significant Global and Local Structural Chemical Features of the $Sr_m[Al_{1-x}Au_x]_{3n}Au_{2(m+n)}$ Phases Identified in This Study: I, I*, II, III, and IV

		I	I*	II	III	IV
refined comp.		$SrAl_{2.94}Au_{4.06(1)}$	$SrAl_{2.54}Au_{4.46(1)}$	$SrAl_{1.95}Au_{5.05(1)}$	$Sr_2Al_{1.67}Au_{7.32(2)}$	$Sr_2Al_{2.82}Au_{6.18(1)}$
at % Sr		12.5	12.5	12.5	18.2	18.2
$\langle V \rangle$ (Å^3/atom)		19.05	19.25	20.04	20.96	20.35
$\langle V_{atom} \rangle$ (Å^3)		21.68	21.69	21.71	23.95	23.93
vec (e^-/atom*)		2.13	2.01	1.84	1.81	2.07
⟨Au−Au⟩ (Å)		2.914	2.924	2.964	2.923	2.894
Au−Au (Å)	Intra 6^3	2.954−3.009	2.999−3.004	2.916−3.117	2.839−3.605	2.881−3.011
	Bet. 6^3	2.869, 2.904	2.850, 2.954	2.800, 3.047	2.968, 2.993	2.979
M−M (Å)	M−Al	2.609, 2.671	2.451, 2.766	2.504−2.666	2.647	2.576
	Al−Al	3.035	2.980	2.972	2.756	
M−Au (Å)	M = Au	2.604−2.853	2.708−2.837	2.827−2.957	2.765−3.005	2.603−2.771
	M = Al	2.553−2.666	2.556−2.647	2.562−2.868	2.603−2.883	

The four compounds **I**−**IV** belong to an emerging homologous series of polar intermetallic compounds with the general formula $Ae_m[M_3]_nAu_{2(m+n)}$ (*Ae* = alkaline-earth and *M* = trielide or tetrelide element) that contain two structural motifs: (*i*) a 3-d tetrahedral Au-framework similar to hexagonal diamond; and (*ii*) single *Ae* atoms and M_3-triangles, each encapsulated within the distorted hexagonal prismatic cavities of the Au-framework (*i*), as shown in Figure 2. Motif (*i*) involves hexagonal rings of Au atoms in a chair conformation fused at each edge into puckered layers. These layers stack so that the hexagons are eclipsed (see Figure 2), and Au−Au connections form between layers so that each Au atom has a distorted tetrahedral coordination by four Au neighbors. For motif (*ii*), depending on the relative atomic proportions *m* and *n*, the M_3-triangles can be either isolated or interconnected into zigzag chains or incomplete Kagomé nets. The complexity and symmetry of these structures depends primarily on changes occurring in the M_3-triangles. As the overall Au content increases, Au atoms replace Al atoms in these triangles, which are essentially $[Al_3]$ entities in the hexagonal and rhombohedral phases **I**, **I***, and **IV**, and the number of Au−Al contacts increases, distances which are normally shorter than Al−Al ones. Consequently, structural deformations caused by the Au−Al shortenings within $[Al_{1-x}Au_x]_3$-triangles are also echoed in the rest of the crystal structure, especially via distortion of the tetrahedral Au-framework (*i*). Reduction of crystalline symmetry from hexagonal and rhombohedral to orthorhombic and monoclinic certainly corresponds with structural distortions caused by Au in substructure (*ii*), but it is also regulated by other factors such as relative atomic proportions, which affects the valence electron concentration, as well as the distribution and condensation of M_3-triangles throughout the voids of the tetrahedral Au-framework. In the next few paragraphs the four structures are described to emphasize their similarities and differences.

In hexagonal $SrAl_{3-x}Au_{4+x}$ the unit cell contains two puckered layers of hexagonal Au rings (6*c* sites) that are situated around $z = 1/4$ and 3/4. The motif (*ii*) of M_3-triangles and Sr atoms involves two different layers: (1) 1 Sr atom: 2 M_3-triangles per unit cell located at $z = 0$; and (2) 2 Sr atoms: 1 Al_3-triangle per unit cell at $z = 1/2$. Mixed Au/Al occupancies occur within the M_3-triangles in the $z = 0$ plane, and these are interconnected at every M site to form a $3(12)^2$ planar net that arranges in an incomplete Kagomé net. The range of refined occupancies for this site, 77.0(3)% Al in **I*** to 96.8(6)% Al in **I**, creates a statistical distribution of $[Al_{3-n}Au_n]$-triangles that extends between ∼87% $[Al_2Au]$ and $[Al_3]$ at the Au-rich end and ∼99% $[Al_2Au]$ and $[Al_3]$ at the Al-rich end. In contrast, the M_3-triangles in the layer at $z = 1/2$ are exclusively $[Al_3]$ and isolated, surrounded by six coplanar Sr atoms. The resulting structural chemical formulation of these phases is $Sr_3[Al_{3-\delta}Au_\delta]_2[Al_3]Au_{12} = Sr_3Al_{9-2\delta}Au_{12+2\delta}$, which establishes its relationship with the hexagonal structure (*hP*24) of $Ba_3Ag_{14.6}Al_{6.4}$.[64]

In the crystal structure **II** of orthorhombic $SrAl_{2-y}Au_{5+y}$, the tetrahedral Au-framework also involves two puckered honeycomb nets, but at $y = 0$ and $y = 1/2$ connected along the *b*-axis. Planes of equal numbers of Sr atoms and M_3-triangles at $y = 1/4$ and $y = 3/4$ are equivalent, related to each other by glide reflections. Each M_3-triangle refines as an averaged composition of $[Al_{1.95}Au_{1.05}]$, but the specific site occupancies identify, in fact, ∼95% $[Al_2Au]$ and ∼5% $[AlAu_2]$ triangles. These triangles form zigzag chains along the *a*-axis exclusively via Au−Al contacts. The resulting formulation of **II** is $Sr[Al_{1.95}Au_{1.05(1)}]$-$Au_4 = Sr_3Al_{1.95}Au_{5.05(1)}$.

Monoclinic $Sr_2Al_{2-z}Au_{7+z}$ (**III**), which exhibits the most distorted tetrahedral Au-network, also has equivalent planes of M_3-triangles and Sr atoms, but in the molar ratio of 1:2. In fact, these planes resemble the motif at $z = 1/2$ in crystal **I**, in which the M_3-triangles are isolated from each other, surrounded completely by Sr atoms. Site occupancy factors for the sites of the M_3-triangle in **III** give an averaged composition $[Al_{1.68}Au_{1.32}]$, i.e., 44% Au, but the refined distribution of Au and Al atoms suggests a statistical distribution of clusters as 3.1% $[Au_3]$, 28.5% $[AlAu_2]$, 65.7% $[Al_2Au]$, and 2.7% $[Al_3]$. The resulting formulation is $Sr_2[Al_{1.68}Au_{1.32}]Au_6 = Sr_2Al_{1.68}Au_{7.32}$.

Rhombohedral $Sr_2Al_{3-w}Au_{6+w}$ (**IV**) also contains equivalent planes of isolated Al-rich M_3-triangles surrounded by Sr atoms, so that it can be formulated as $Sr_2[Al_{2.82}Au_{0.18}]Au_6 = Sr_2Al_{2.82}Au_{6.18}$. There are six puckered hexagonal nets of Au atoms stacked along the *c*-axis with three distinct channels of voids occupied by ···Sr···$[Al_{2.82}Au_{0.18}]$···Sr···. This structure type has been recently reported for *Ae*−*T*−Au phases (*Ae* = Sr, Ba; *T* = Zn,Cd,...).[65,66]

Volume and Coordination Analyses. Since the four structures **I**−**IV** all adopt a similar hexagonal diamond-like, tetrahedral Au-framework and achieve their stoichiometric diversity from both the compositions of the $[Al_{1-x}Au_x]_3$-triangles and the ratio between Sr atoms and these triangles, an examination of some local and global structural trends is warranted. Some global characteristics, viz., average atomic

dx.doi.org/10.1021/ja411150e | J. Am. Chem. Soc. 2014, 136, 3108−3117

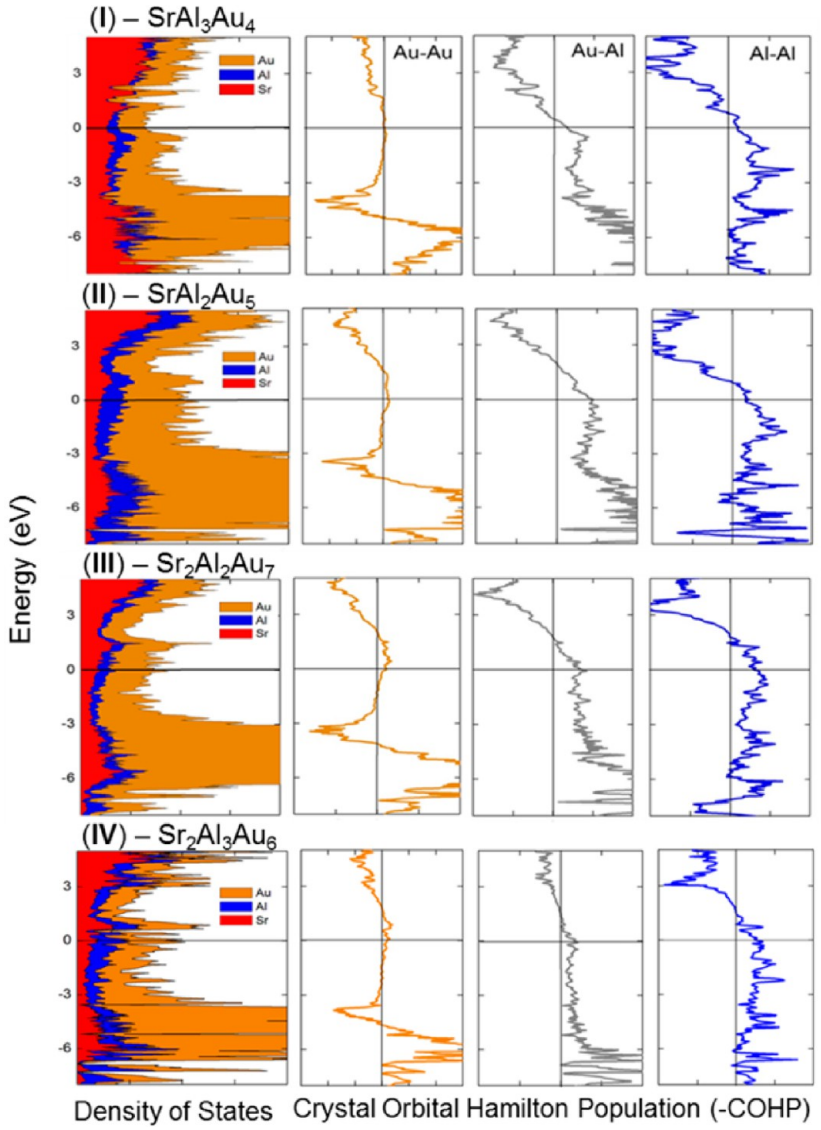

Figure 3. DOS and Au−Au, Au−Al, Al−Al COHP curves for models of the four crystal structures **I**, **II**, **III**, and **IV** as described in the text. The Fermi levels for each structure are the reference energy levels. Total DOS curves (left) have individual contributions from Sr (red), Au (gold), and Al (blue) indicated.

volume, average Au−Au distance in the tetrahedral net, and average valence electron count per electronegative element Au +Al, for samples **I**, **I***, **II**, **III**, and **IV** are summarized in Table 3. Room temperature densities of the elements Sr, Au, and Al give their approximate atomic volumes, respectively, as 56.0, 16.9, and 16.6 Å^3. In combination, the four compounds yield ∼10−12% contraction of the average atomic volume, which partially substantiates their classification as polar intermetallic compounds. The results in Table 3 identify two distinct categories: (a) two cases **I**, **I***, and **IV** with *vec* = 2.01−2.13 and primarily [Al_3]-triangles; and (b) two cases **II** and **III** with *vec* = 1.81−1.84 and primarily [Al_2Au]-triangles.

Although the average volume per atom increases with increasing Au and Sr content, the average Au−Au distances in the hexagonal diamond-like tetrahedral framework vary between 2.894 Å in **I** and 2.964 Å in **III**. The symmetry of this motif is significantly disrupted by the nature of the M_3-triangles occupying the voids. Among all four structures, the most regular motif (*i*) occurs in hexagonal $SrAl_{3-x}Au_{4+x}$ **I** and **I***. For example, the Au−Au distances within puckered hexagons are similar and comprise narrow ranges, i.e., ∼2.98−3.00 Å in **I** and ∼2.95−3.01 Å in **I***. The structural response of the hexagonal diamond network of Au atoms on increasing Au content in $SrAl_{3-x}Au_{4+x}$ is greater for Au−Au separations between the hexagonal layers. These Au−Au separations already depend on how the void spaces between hexagonal layers are filled: if the space is filled by the incomplete Kagomé net of M_3-triangles, the Au−Au contacts are shorter (∼2.87 Å) than if it is filled by isolated Al_3-triangles (∼2.90 Å). This difference becomes more pronounced in the Au-rich specimen **I***, in which the additional Au atoms are introduced solely into M_3-units of the incomplete Kagomé nets rather than into the isolated triangles.

The hexagonal diamond-like motif (*i*) is even more distorted in the Au-richer orthorhombic $\mathbf{SrAl_{2-y}Au_{5+y}}$ and monoclinic $\mathbf{Sr_2Al_{2-z}Au_{7+z}}$. In these two phases the voids between pseudohexagonal Au layers are filled by equivalent motif (*ii*) units. Strikingly, though, the locations of all long Au−Au distances in submotif (*i*) correspond to the location of the Au atom in [AlMAu]-triangles of submotif (*ii*). The presence of Au

dx.doi.org/10.1021/ja411150e | J. Am. Chem. Soc. 2014, 136, 3108−3117

atoms as a distinct crystallographic position in the M_3-triangles introduces local repulsions between neighboring Au atoms of the hexagonal rings, whereas the remaining two atoms of these triangles, which are primarily Al, retain more attractive heteroatomic Au−Al interactions and, thereby, shorter distances.

Electronic Structure and Bonding Analysis. Although the crystal structures of the title compounds showed some mixed Au/Al occupancies among sites in the M_3-triangles, for the TB-LMTO-ASA calculations, all sites were assigned to their majority element resulting in four idealized compositions: hexagonal "$SrAl_3Au_4$", orthorhombic "$SrAl_2Au_5$", monoclinic "$Sr_2Al_2Au_7$", and rhombohedral "$Sr_2Al_3Au_6$". As mentioned above, these four compounds fall into two distinct classes according to their valence electron count per electronegative (Au+Al) element. This electron counting approach does not include the valence 5*d* electrons of Au because these valence orbitals are formally filled and located in a broad band that is located ∼3−7 eV below the corresponding Fermi levels in the DOS curves. Nevertheless, the Au 5*d* orbitals do participate in chemical bonding with both empty Sr 4*d* and Al 3*p* wave functions. The influence of Au 5*d* orbitals on the 6*s* and 6*p* valence orbitals and their participation in bonding has been discussed,[41] and is closely associated with relativistic effects associated with Au.

The similarities among crystal structures **I**, **II**, **III**, and **IV** translate into similar DOS curves for the model compositions (see Figure 3). In line with typical polar intermetallic compounds containing a late transition metal, all DOS curves generally show a wide *s* and *p* valence band, which is intersected by the 5*d* band of Au and reveals deviations from free-electron-like characteristics near the corresponding Fermi levels. Often, polar intermetallic compounds will have a pseudogap in the DOS curve close to the corresponding Fermi levels. In these Sr−Al−Au cases, however, the pseudogaps in the DOS curves lie above all respective Fermi levels. From the individual atomic contributions to the DOS curves, the Fermi levels correspond to the regions where Sr contributions begin to increase.

The analyses of crystal orbital Hamilton populations (COHP), which provide a measure of covalent bonding interactions in chemical structures, also exhibit some unusual features for these polar intermetallics. In hexagonal "$SrAl_3Au_4$", with the highest valence electron concentration per electronegative metal (e/a = 2.14) and lowest Au content (50 at. %), the heteroatomic Au−Al contacts contribute the most to the total Hamilton population (∼63%) by having both the largest −ICOHP values (averaging 1.65 eV/bond) and being the most frequently occurring interactions (54 contacts/cell) in the structure. However, the Au−Al orbital interactions are not optimized at E_F suggesting that some electron-richer atoms, such as additional Al atoms, could be introduced into the structure so that additional valence electrons could occupy the remaining Au−Al bonding states. In $SrAl_{3-x}Au_{4+x}$, however, the opposite situation occurs, i.e., Au atoms replace Al atoms at the 4*c* sites, an outcome that lowers the total valence electron count and must deplete Au−Al bonding orbitals. On the other hand, additional Au atoms will decrease the number of Al−Al contacts within the triangles, replacing them by strong polar covalent Au−Al interactions, and also increasing the number of Au−Au contacts. The latter interactions are especially important in structural stabilization of "$SrAl_3Au_4$", considering their significant contribution to the total Hamilton population (∼17%), which comes as a result of their significant number (of total 24), as well as large −ICOHP values, which are, on average, ∼1.03 eV/bond (see Tables S4−S6 in SI).

Perhaps the most interesting features emerging from the analysis of all COHP curves are the broad, nonbonding regions of Au−Au interactions located from ∼3 eV below to ∼1.5 eV above the Fermi levels in all four structures. Thus, both addition and subtraction of valence electrons should not significantly disrupt the 3-d tetrahedral Au-framework until these critical energy values are reached. Therefore, two questions immediately arise: (1) whether the 3-d tetrahedral Au-framework can exist without any trielide structural component in the voids; and (2) whether the role of the trielide element can be played exclusively by Au atoms, so that all triangles in the prismatic voids are built up of only Au atoms. A partial resolution for both questions can be found by analyzing the Sr−Au binary system, specifically the crystal structures of $SrAu_2$ and $SrAu_5$. $SrAu_2$[67] does not crystallize in the hexagonal $CaIn_2$-type structure, but adopts the orthorhombic $CeCu_2$-type structure,[68] in which every Au atom is coordinated by a distorted tetrahedral environment of four Au atoms. Although $CeCu_2$-type $SrAu_2$ also contains distorted, puckered hexagonal nets of Au atoms, these layers are stacked to create four-membered rings rather than six-membered rings in the boat conformation found in the $CaIn_2$-type structure. $SrAu_5$,[69] which adopts the hexagonal $CaCu_5$-type structure, reveals that additional Au atoms can form triangular units, but these will rather condense together with Au-hexagons into Kagomé-like nets rather than retain a 3-d tetrahedral framework. Another example, $Mg_{13}Au_{41}$,[70] shows that [Au_3]-triangles can center hexagonal Au prisms, but without any obvious bonding features between two Au-hexagons. Therefore, from this brief structural−chemical analysis, we conclude that the presence of Al is essential to stabilize the 3-d tetrahedral, hexagonal, diamond-like Au-framework. The existence of this network in this series of Sr−Al−Au compounds suggests that Au is similar to trielide or tetrelide elements, which form such tetrahedral frameworks as either formally negatively charged (trielides) or neutral (tetrelide) species, as it is known from intermetallic clathrates.[71] Thus, gold atoms use their valence 6*s* and 6*p* orbitals for covalent interactions with aluminum within the net. From the DOS and Au−Au COHP curves, the filled 5*d* orbitals contribute minimally to bonding within the Au tetrahedral framework. The Au−Au interaction within the network is not very strong (cf. ICOHP values in Tables S4−S7 in SI). The existence of $Ba_3Ag_{14.6}Al_{6.4}$,[64] which contains a hexagonal diamond-like Ag-framework, is another similar example, in which the filled 4*d* bands of Ag are located lower in energy (see Figure S3 in SI), and show lower dispersion, i.e., are more localized, than the 5*d* bands of Au in $SrAl_{3-x}Au_{4+x}$.

Further insights into the structural organization and chemical bonding features of these gold-rich compounds in the Sr−Al−Au system were obtained by analysis of atomic interactions in real space using the electron localizability approach.[58] According to the absolute electronegativity values of the components[72] (Au, 5.77; Al, 3.23; Sr, 2.00), a formal anionic behavior of the gold atoms, significant polar character of Al−Au interactions, as well as a formal cationic behavior of the embedded Sr atoms may be expected. This expectation is supported by the atomic charges calculated according to QTAIM.[60] The shapes of the QTAIM atomic basins together with the effective charges in "$SrAl_2Au_5$" (**II**) are shown in Figure 4; the effective charges for all four model compounds are collected in Table 4. The atomic basins of Sr have shapes that

dx.doi.org/10.1021/ja411150e | J. Am. Chem. Soc. 2014, 136, 3108−3117

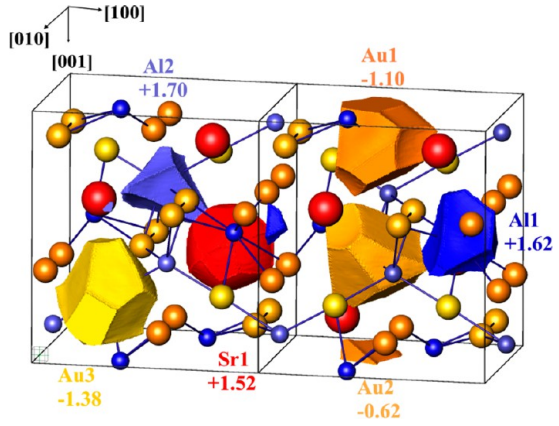

Figure 4. QTAIM atomic basins and effective charges in orthorhombic $SrAl_2Au_5$, which is a model for phase **II**. Perspective view along the *b*-axis. Two unit cells are depicted.

Table 4. Effective Charges from the QTAIM Atomic Basins of the Sr−Al−Au Model Compounds for I−IV

atoms	"$SrAl_3Au_4$" (I)	"$SrAl_2Au_5$" (II)	"$Sr_2Al_2Au_7$" (III)	"$Sr_2Al_3Au_6$" (IV)
Sr1	+1.39	+1.52	+1.44	+1.45
Sr2	+1.54			
Al1	+1.21	+1.62	+1.45	+1.27
Al2	+1.26	+1.70		
Au1	−1.29	−1.10	−0.93	−1.11
Au2	−1.30	−0.62	−0.57	
Au3		−1.38	−1.03	
Au4			−0.70	

are nearly spherical and include the inner four shells. The valence fifth shell is completely missed, which might be expected assuming their role as cations and charge transfer to the polyanionic framework, cf., for example, Sr in $Sr_8Al_6Si_{40}$[73] or Mg in MgB_2[74]). Integration of the electron density within each Sr atomic basin yields effective charges of +1.4−1.5, values that are very close to those recently observed for Sr in $Sr_8Al_6Si_{40}$.[73] On the other hand, the basins of Al and Au are not spherical and resemble the coordination of these atoms in the crystal structure. They include also the valence shells. Such features of atomic basins of Al and Au indicate significant covalency to the Al−Au interactions. Because the QTAIM charges for aluminum atoms are positive, the aluminum−gold interaction has significant polar character. The relatively large charge differences between different Au sites may be understood in connection with their local coordination. Whereas the slightly negatively charged Au2 sites are surrounded by 6 electropositive (3Sr + 3Al) and 2 electronegative Au atoms, the Au3 species, which carry the largest negative charge, are surrounded by 6 electropositive (3Sr + 3Al) and 5 electronegative gold atoms; the Au1 sites with the intermediate charge have just 5 electropositive (3Sr + 2Al) and 3 electronegative Au atom neighbors. The amount of negative charge on the Au atoms changes with the number of the (negatively charged) homonuclear neighbors. Thus, in general, charge transfer plays an important role in the organization of the crystal structure of "$SrAl_2Au_5$," as well as in all model Sr−Al−Au structures studied here. Although the larger unit cells and numbers of atoms per cell hinder evaluation of more precise populations of the atomic basins, a slight tendency of the dependence of charge transfer on the Au:(Sr + Al) ratio is suggested from the effective charges in Table 4.

The atomic interactions in "$SrAl_2Au_5$" were analyzed using the electron localizability approach.[58] The distribution of the ELI around each Sr nucleus is spherical and does not reveal its valence shell; there are no dedicated ELI-D maxima in the space between Sr and any atoms in its environment (see Figure 5, top). This outcome agrees well with the cationic behavior of

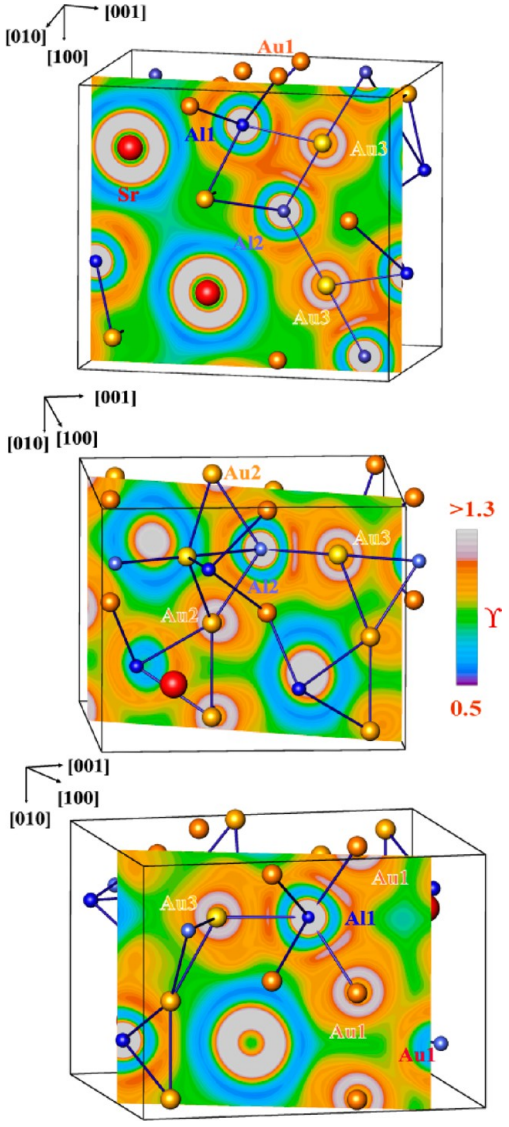

Figure 5. Electron-Localizability-Indicator in "$SrAl_2Au_5$": (top) ELI-D distribution in the plane of Al1−Al2−Au3 triangles; (middle) ELI-D distribution in the plane of Al2−Au2 and Al2−Au3 bonds; (bottom) ELI-D distribution in the plane of Al21−Au1 and Al1−Au3 bonds.

Sr in "$SrAl_2Au_5$." Now, a special feature of all Sr−Al−Au compounds studied here is formation of $[Al_3]$- or $[Al_2Au]$-triangles sandwiched between the corrugated six-rings formed by Au atoms (see Figure 2). In "$SrAl_2Au_5$," these triangles are heteroatomic $[Al_2Au]$-type and are interconnected in the ***ac***-plane to form ribbons (see Figure 2, **II**). Despite the relatively short Al−Al distance (2.97 Å), the ELI-D does not show any direct Al−Al interaction, although there is clearly Al−Au bonding in the triangle (Figure 5, top). In addition, each Al atom participates in Al−Au interactions above and below the

dx.doi.org/10.1021/ja411150e | *J. Am. Chem. Soc.* 2014, 136, 3108−3117

plane of the [Al_2Au]-triangle. These interactions have mainly two-center character but show a distinct tendency toward three-center character also (Figure 5, middle and bottom). The local interactions involving Al are similar to those observed in Al_2Cu,[75] in which three-bonded Al atoms form interpenetrating graphite-like planes. Furthermore, in "$SrAl_2Au_5$," no dedicated ELI-D attractors were found for the Au−Au contacts despite their relatively short distances, a result that is in agreement with the nonbonding Au−Au interactions around the Fermi level deduced from the COHP analysis (cf. above) and may be caused by the fact that Au atoms participate in the three-center interactions with Al. On-going investigations to shed more light on this somewhat unusual result are in progress.

Despite the similarities among the triangular units in the four crystal structures **I**−**IV**, the interatomic interactions within them will be very sensitive to the local atomic coordination. For example, in the crystal structure of $SrAl_{3-x}Au_{4+x}$, two types of triangular clusters are present. In the z = 0 and related planes (Figure 6, top), the two-center Al−Al interactions in the triangle are more pronounced, while the interactions below and above the triangle's plane have more three-center character. In the z = 1/2 and related planes, the distribution of ELI-D indicates a rather weak Al−Al interaction within the triangle, as in the F_2 molecule[58] with more pronounced two-center character of the Al−Au bonds above and below each triangle's plane. In "$Sr_2Al_2Au_7$," the two-center Al−Al interactions within the [Al_2Au]-triangle are supported by Al−Au bonding out of the plane. No dedicated ELI-D maxima are found along the Al−Au contacts within the triangle (Figure 6, middle). Lastly, the Al atoms in "$Sr_2Al_3Au_6$" engage in mostly two-center Al−Al interactions within the [Al_3]-triangle followed by the predominantly two-center Al−Au interactions above and below the triangles (Figure 6, bottom).

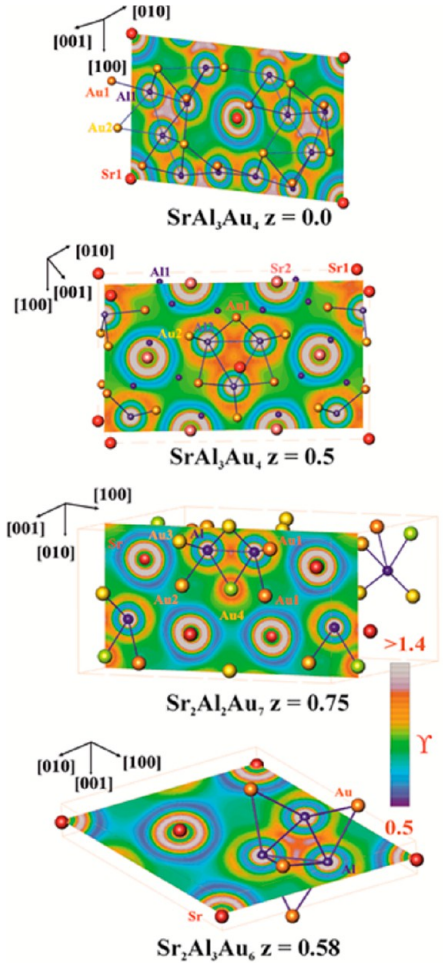

Figure 6. Interatomic interactions within the [Al_3]- or [Al_2Au]-triangles in "$SrAl_3Au_4$" (top; z = 0 and z = 1/2), "$Sr_2Al_2Au_7$" (middle; z = 3/4), and "$Sr_2Al_3Au_6$" (z = 0.58).

SUMMARY

Four new compounds in the Sr−Al−Au system with the general formulation $Sr_m[Al_{1-x}Au_x]_{3n}Au_{2(m+n)}$ have been discovered using high-temperature synthetic approaches. All four compounds adopt structures that contain Au atoms in a 3-d tetrahedral framework that resembles the structure of a hexagonal diamond. The corresponding hexagonal prismatic voids contain either a Sr atom, which shows cationic behavior from analyses of their electronic structures, or an [Al_3]- or [Al_2Au]-triangle. Bonding within the structures is dominated by polar-covalent 2-center and 3-center Al−Au interactions within the anionic Al−Au framework built of the two distinct motifs, i.e., the 3-d tetrahedral Au-framework and the triangles. Surprisingly, the Au−Au orbital interactions are nonbonding around the corresponding Fermi levels and are also not deduced from the electron localizability approach.

ASSOCIATED CONTENT

Supporting Information

Results of phase analyses illustrated in Figure 1, powder X-ray diffraction patterns for phases **I**−**IV** as well as for runs (4−8), single-crystal refinement data and structural parameters for crystal **I***, selected interatomic distances and −ICOHP values for **I**, **II**, and **III**, electronic DOS of hexagonal $Ba_3Ag_{12}Al_9$, plus the refinement parameters of crystals **I**, **II**, **III**, and **IV** in CIF format. This material is available free of charge via the Internet at http://pubs.acs.org.

AUTHOR INFORMATION

Corresponding Author

gmiller@iastate.edu

Notes

The authors declare no competing financial interest.

ACKNOWLEDGMENTS

The research was supported by the U.S. National Science Foundation via NSF DMR 10-05765. The computations were done on the CRUNCH system supported by Iowa State University Computation Advisory Committee project 202-17-10-08-0005. Y.G. appreciates the fruitful discussion and support of M. Kohout and F. R. Wagner.

REFERENCES

(1) Miller, G. J.; Lee, C. −S.; Choe, W. In *Inorganic Chemistry Highlights*; Meyer, G., Naumann, D., Wesemann, L., Eds.; Wiley-VCH: Weinheim, Germany, 2002; pp 21 − 53.
(2) Corbett, J. D. *Chemistry, Structure and Bonding of Zintl Phases and Ions*; Kauzlarich, S., Ed; VCH Publishers: New York, 1996.
(3) Corbett, J. D. *Angew. Chem., Int. Ed.* **2000**, *39*, 670.
(4) Schäfer, H.; Eisenmann, B.; Müller, V. *Angew. Chem., Int. Ed.* **1973**, *12*, 683.
(5) Nesper, R. *Angew. Chem., Int. Ed.* **1991**, *30*, 189.
(6) Hume-Rothery, W. *J. Inst. Met.* **1926**, *35*, 295.

(7) Hume-Rothery, W.; Raynor, G. V. *The Structure of Metals and Alloys*, 4th ed.; Institute of Metals: London, U.K., 1962.
(8) (a) Wade, K. *J. Chem. Soc. D, Chem. Commun.* **1971**, 792. (b) Wade, K. *Adv. Inorg. Chem. Radiochem.* **1976**, *18*, 1.
(9) (a) Mingos, D. M. P. *Nat. Phys. Sci.* **1972**, *236*, 99. (b) Mingos, D. M. P. *J. Chem. Soc. Chem. Commun.* **1983**, 706.
(10) Mizutani, U. *Hume-Rothery Rules for Structurally Complex Alloy Phases*; CRC Press: Boca Raton, 2011.
(11) Palasyuk, A.; Dai, J.-C.; Corbett, J. D. *Inorg. Chem.* **2008**, *47*, 3128.
(12) Palasyuk, A.; Corbett, J. D. *Inorg. Chem.* **2008**, *47*, 9344.
(13) Li, B.; Corbett, J. D. *Inorg, Chem.* **2008**, *47*, 3610.
(14) Hoffmann, R.-D.; Pöttgen, R.; Rosenahn, C.; Mosel, B. D.; Künnen, B.; Kotzyba, G. *J. Solid State Chem.* **1999**, *145*, 283.
(15) Muts, I.; Schappacher, F. M.; Hermes, W.; Zaremba, V. I.; Pöttgen, R. *J. Solid State Chem.* **2007**, *180*, 2202.
(16) Muts, I.; Rodewald, U. Ch.; Zaremba, V. I.; Pöttgen, R. *Z. Naturforsch.* **2011**, *66b*, 1101.
(17) Li, B.; Corbett, J. D. *Inorg. Chem.* **2007**, *46*, 6022.
(18) Sinnen, H. D.; Schuster, H. U. *Z. Naturforsch.* **1978**, *33b*, 1077.
(19) Schwarz, U.; Schmidt, M.; Gumeniuk, R.; Schnelle, W.; Hanfland, M.; Klementiev, K.; Grin, Yu. *Z. Anorg. Allg. Chem.* **2004**, *630*, 122.
(20) Sichevych, O.; Kohout, M.; Schnelle, W.; Borrman, H.; Cardoso-Gil, R.; Schmidt, M.; Burkhardt, U.; Grin, Yu. *Inorg. Chem.* **2009**, *48*, 6261.
(21) Lin, Q.; Corbett, J. D. *J. Am. Chem. Soc.* **2007**, *129*, 6789.
(22) Gumeniuk, R.; Akselrud, L.; Kvashnina, K. O.; Schnelle, W.; Tsirlin, A. A.; Curfs, C.; Rosner, H.; Schoeneich, M.; Burkhardt, U.; Schwarz, U.; Grin, Yu.; Leithe-Jasper, A.. *Dalton Trans.* **2012**, *41*, 6299.
(23) Gumeniuk, R.; Sarkar, R.; Geibel, C.; Schnelle, W.; Paulmann, C.; Baenitz, M.; Tsirlin, A. A.; Guritanu, V.; Sichelschmidt, J.; Grin, Yu.; Leithe-Jasper, A. *Phys. Rev. B* **2012**, *86*, 235138.
(24) Gumeniuk, R.; Borrmann, H.; Ormeci, A.; Rosner, H.; Schnelle, W.; Nicklas, M.; Grin, Yu.; Leithe-Jasper, A. *Z. Kristallogr.* **2010**, *225*, 531.
(25) Zachwieja, U. *J. Alloys Compd.* **1996**, *235*, 7.
(26) Zachwieja, U.; Wlodarski, J. *Z. Anorg. Allg. Chem.* **1998**, *624*, 1443.
(27) Zachwieja, U.; Wlodarski, J. *Z. Anorg. Allg. Chem.* **1995**, *621*, 975.
(28) Zachwieja, U.; Wlodarski, J. *Z. Anorg. Allg. Chem.* **1998**, *624*, 1569.
(29) Li, B.; Kim, S.-J; Miller, G. J.; Corbett, J. D. *Inorg. Chem.* **2009**, *48*, 11108.
(30) Lin, Q.; Corbett, J. *Inorg. Chem.* **2007**, *46*, 8722.
(31) Li, B.; Kim, S.-J.; Miller, G. J.; Corbett, J. D. *Inorg. Chem.* **2010**, *49*, 1503.
(32) Li, B.; Kim, S.-J.; Miller, G. J.; Corbett, J. D. *Inorg. Chem.* **2009**, *48*, 6573.
(33) Lin, Q.; Corbett, J. *Inorg. Chem.* **2011**, *50*, 1808.
(34) Muts, I.; Matar, S. F.; Rodewald, U. Ch.; Zaremba, V. I.; Pöttgen, R. *Z. Naturforsch.* **2011**, *66b*, 993.
(35) Smetana, V.; Lin, Q.; Pratt, D. K.; Kreyssig, A.; Ramazanoglu, M.; Corbett, J. D.; Goldman, A. I.; Miller, G. J. *Angew. Chem., Int. Ed.* **2012**, *51*, 12699.
(36) Lin, Q.; Smetana, V.; Miller, G. J.; Corbett, J. D. *Inorg. Chem.* **2012**, *51*, 8882.
(37) Smetana, V.; Miller, G. J.; Corbett, J. D. *Inorg. Chem.* **2012**, *51*, 7711.
(38) Smetana, V.; Corbett, J. D.; Miller, G. J. *Inorg. Chem.* **2012**, *51*, 1695.
(39) Pyykkö, P. *Chem. Rev.* **1988**, *88*, 563.
(40) Pearson, R. G. *Inorg. Chem.* **1988**, *27*, 734.
(41) Miller, G. J.; Thimmaiah, S.; Smetana, V.; Palasyuk, A.; Lin, Q. *Proc. Mater. Res. Soc.* **2013**, 1517.
(42) Cordier, G.; Doersam, G.; Roehr, C. *J. Less-Common Met.* **1990**, *166*, 115.
(43) Cordier, G.; Friedrich, T. *Z. Kristallogr.* **1992**, *201*, 304.
(44) Cordier, G.; Friedrich, T. *Z. Kristallogr.* **1992**, *201*, 306.
(45) Hulliger, F.; Nissen, H. U.; Wessicken, R. *J. Alloys Compd.* **1994**, *206*, 263.
(46) Corbett, J. D. *Inorg. Synth.* **1983**, *22*, 15.
(47) *STOE WinXpow*, 2.10; STOE & Cie GmbH: Darmstadt, Germany, 2004.
(48) *SMART*; Bruker AXS, Inc.; Madison, WI, 1996.
(49) *SHELXTL*; Bruker AXS, Inc.; Madison, WI, 2000.
(50) Blessing, R. H. *Acta Crystallogr.* **1995**, *A51*, 33.
(51) Jepsen, O.; Burkhardt, A.; Andersen, O. K. *The Program TB-LMTO-ASA*, 4.7; Max-Planck-Institut für Festkörperforschung, Stuttgart, Germany: 1999.
(52) von Barth, U.; Hedin, L. *J. Phys. C: Solid State Phys.* **1972**, *5*, 1629.
(53) Koelling, D.; Harmon, B. N. *J. Phys. C* **1977**, *10*, 3107.
(54) Andersen, O. K. *Phys. Rev. B: Condens. Matter Mater. Phys.* **1975**, *12*, 3060.
(55) Lambrecht, W. R. L.; Andersen, O. K. *Phys. Rev. B* **1986**, *34*, 2439.
(56) Dronskowski, R.; Blöchl, P. *J. Phys. Chem.* **1993**, *97*, 8617.
(57) Kohout, M. *Int. J. Quantum Chem.* **2004**, *97*, 651.
(58) Wagner, F. R.; Bezugly, V.; Kohout, M.; Grin, Yu. *Chem.—Eur. J.* **2007**, *13*, 5724.
(59) Kohout, M. *Faraday Discuss.* **2007**, 43.
(60) Bader, R. F. W. *Atoms in Molecules, A Quantum Theory*. Clarendon Press and Oxford University Press Inc.: New York, 1994.
(61) Kohout, M. *DGrid*, version 4.6; Radebeul, 2011.
(62) Zintl, E.; Haucke, W. *Z. Elektro. Angew. Phys. Chem.* **1938**, *44*, 104.
(63) Baenziger, N. C.; Conant, J. W. *Acta Crystallogr.* **1956**, *9*, 361.
(64) Cordier, G.; Roehr, C. *J. Less-Common Met.* **1991**, *170*, 333.
(65) Lin, Q.; Mishra, T.; Corbett, J. D. *J. Am. Chem. Soc.* **2013**, *135*, 11023.
(66) Gerke, B.; Hoffmann, R.-D.; Pöttgen, R. *Z. Anorg. Allg. Chem.* **2013**, *639*, 2444.
(67) Zachwieja, U. *J. Alloys Compd.* **1996**, *235*, 12.
(68) Debray, D. *J. Less-Common Met.* **1973**, *30*, 237.
(69) Feller-Kniepmeier, M.; Heumann, T. *Z. Metallkd.* **1960**, *51*, 404.
(70) Burkhardt, K.; Schubert, K.; Toth, R. S.; Sato, H. *Acta Crystallogr. Sect. B* **1968**, *24*, 137.
(71) Zhang, H.; Borrmann, H.; Oeschler, N.; Candolfi, C.; Schnelle, W.; Schmidt, M.; Burkhardt, U.; Baitinger, M.; Zhao, J.-T.; Grin, Yu. *Inorg. Chem.* **2011**, *50*, 1250.
(72) Emsley, J. *The Elements*; Oxford University Press: New York, 1991.
(73) Roudebush, J. H.; Tsujii, N.; Hurtando, A.; Hope, H.; Grin, Yu.; Kauzlarich, S. M. *Inorg. Chem.* **2012**, *51*, 4161.
(74) Tsirelson, V.; Stash, A.; Kohout, M.; Rosner, H.; Mori, H.; Sato, S.; Lee, S.; Yamamoto, A.; Tajima, S.; Grin, Yu. *Acta Crystallogr., Sect. B* **2003**, *B59*, 575.
(75) Grin, Yu.; Wagner, F. R.; Armbrüster, M.; Kohout, M.; Leithe-Jasper, A.; Schwarz, U.; Wedig, U.; von Schnering, H. G. *J. Solid State Chem.* **2006**, *179*, 1707.